Marine Structures 76 (2021) 102915

Contents lists available at ScienceDirect

Marine Structures

journal homepage: http://www.elsevier.com/locate/marstruc

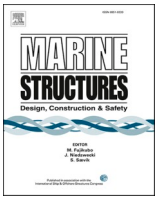

Estimation of natural frequencies and damping using dynamic field data from an offshore wind turbine

Karin Norén-Cosgriff *, Amir M. Kaynia

Norwegian Geotechnical Institute (NGI), Oslo, Norway

ARTICLE INFO

Keywords:
Offshore wind energy
Pile foundation
Measurements
Acceleration
Strain
Natural frequencies
Soil damping

ABSTRACT

The dynamic characteristics of offshore wind turbines are heavily affected by environmental loads from wave and wind action and nonlinear soil behaviour. In the design of the monopile structures, the fatigue load due to wind and wave loading is one of the most important problems to consider. Since the fatigue damage is sensitive to the foundation stiffness and damping, increasing the accuracy of analysis tools used in the design and optimization process can improve the reliability of the structure and reduce conservatism, thereby leading to a more cost-efficient design. In this context, analysis of field data is important for calibrating and verifying purposes. This paper presents analysis of measured accelerations and strains from a wind farm in the North Sea with monopile foundations. Field data during idling conditions, collected over long periods of operation, are analysed and the natural frequencies are determined, and damping is estimated. The measured natural frequencies are compared to calculated values using an aero-servo-hydro-elastic code, showing a good agreement in the frequency range below 2 Hz. Variation of the natural frequencies with intensity of loading may indicate effect of soil nonlinearity on the overall OWT response. Since the first natural bending modes have the largest potential to mobilize soil reactions, they are of primary interest in this context. The effect of load (wave, wind and dynamic bending moment) on the first natural frequency is investigated using different analysis techniques in the frequency domain and time domain. A clear correlation between load level and first natural frequency is demonstrated. A simple nonlinear SSI model of the tower/soil system is employed to numerically investigate the observed changes in the measured first natural frequency with the level of loading and increased overall damping. The simulated results reproduce the general trends in the observed reduction in the first natural frequency and increased damping ratio with the load level. However, the effect of the load level is less than that observed in the measurements, indicating contribution also from other factors than soil nonlinearity.

1. Introduction

For soft-stiff designs, which is the case for the offshore wind turbine (OWT) considered in this study, the first natural frequency is designed to be in the narrow frequency range in between the rotor frequency (1P) and the blade passing frequency (3P). Therefore, it is crucial to obtain a reliable estimation of the first natural frequency in design. According to Ref. [1] soil-structure interaction (SSI)

* Corresponding author.
E-mail address: knc@ngi.no (K. Norén-Cosgriff).

https://doi.org/10.1016/j.marstruc.2020.102915
Received 13 May 2020; Received in revised form 30 September 2020; Accepted 15 November 2020

effects can reduce the fixed-base fundamental frequency of an OWT more than 15% in the frequency range above 0.25 Hz. Therefore, analysis tools need to include an accurate description of the soil. In this context, analysis of field data is important for calibrating and verifying purposes. However, only measurements from a few installations are reported in the literature some of which are mentioned below.

In [2] analyses of more than 1500 "rotor-stop" tests performed on OWTs founded on monopiles in four wind parks are described. In that study, the first natural frequencies and modal damping of the structures were determined from the vibration decay data. Research in Ref. [3] presents results of analyses of measurement data collected over a 2.5 years period from one offshore wind turbine structure on a monopile foundation in Horns Reef II wind farm. It was observed that the pile-soil stiffness was reduced during a major storm event but was completely regained after the storm. In Ref. [4] results are presented from analyses of 'rotor stop' tests performed on one offshore wind turbine on a monopile in Burbo Banks wind farm. The first natural frequencies and damping were determined from the vibration decay data. Studies carried out in Refs. [5] report results from a load measuring campaign on one offshore wind turbine on a monopile in Horns Rev 1 Wind Farm. Bending moments were calculated from measured strain and were compared with coinciding environmental data (wind, wave and current). The results were compared to traditional design methodologies for offshore wind farms using p-y springs for the soil. It was observed that the soil was significantly stiffer than represented by p-y springs. The research work in Ref. [6] reports measurements of overall damping from "rotor-stop" test in the Horns Rev 1 and the Burbo offshore wind farms. A theoretical reconstruction was made to estimate the individual contributions to the overall damping from soil, hydrodynamics, structure and tower dampers, and it was shown that the soil is the main contributor to the overall damping of the first mode. Finally, [7, 8] present data from a long-term monitoring campaign and overspeed stops performed at the Belwind wind farm. Natural frequencies and damping were obtained from decay rate and by using operational modal analysis techniques. The results were further compared to calculation values.

In the present study, analyses of measurement data from a wind farm in the North Sea with monopile foundations are presented. Measured acceleration and strain data collected over several periods of idling conditions are analysed. The objectives of these analyses are twofold. First, to determine the natural frequencies and damping to be used in validation of a developed foundation model, and second, to observe any sensitivity of these data to the intensity of loading, which in turn may point to the role of soil nonlinearity. Since the first natural bending modes have the largest potential to mobilize soil reactions, they are of primary interest in this context. This paper describes the analyses performed together with the main results and findings.

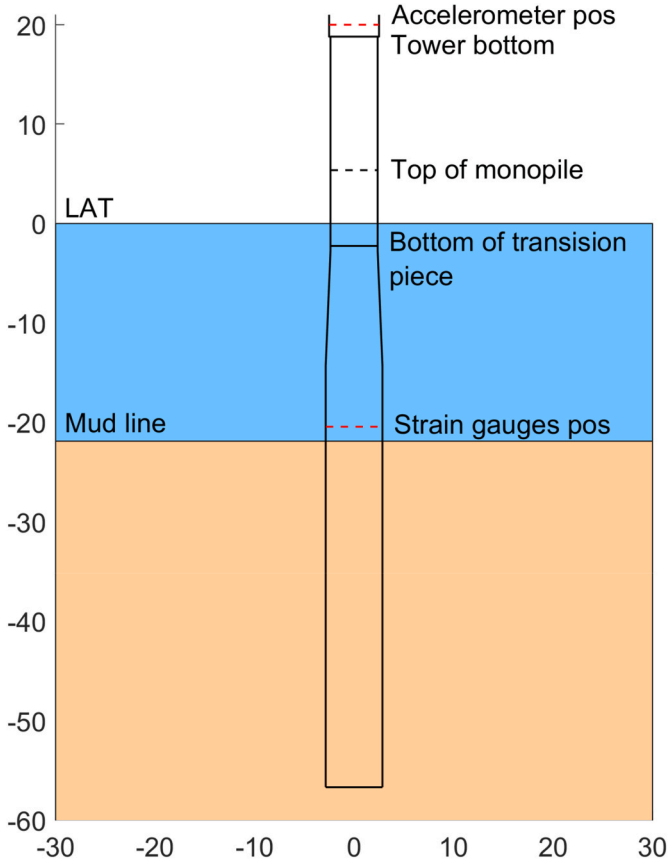

Fig. 1. Monopile layout and sensor location.

2. Site condition, OWT structure and instrumentation

The wind farm in this study, is in a predominantly clay site in the North Sea with more than 80 3.6 MW wind turbines. Measurement data from one of the turbines are used in this study. The monopile has the following dimensions, diameter 5.70 m, length 28 m, thickness 50–70 mm, weight 477 tonnes. The water depth is 22 m. The total weight of transition piece, tower, turbine and blades is 890 tonnes. No indication of scouring has been reported at this site.

The tower is equipped with horizontal and vertical accelerometers close to the tower base together with strain gauges at several levels in the tower, the transition piece and the monopile. Four strain gauges are located about evenly distributed over the circumference at each level. In the present study, measured accelerations in horizontal X- and Y-direction at tower base, and foundation vertical strain are analysed. One of the strain gauges at the foundation level did not work. Therefore, the analysis is based on three strain sensors in the positions 10°, 100° and 280° to North. In addition, information about wind speed, wind direction, and turbine power production are used. All data are logged synchronously with 25 Hz sampling frequency. Information about wave height and wave direction are collected from a nearby metmast. Fig. 1 shows the monopile and the location of the analysed accelerometer and strain gauges.

Assessment of load, i.e. through dynamic bending moment, is based on measured strain as described in section 3.2. The determination of natural frequencies and damping are based on acceleration, since these data have the best quality.

3. Data used in the analyses

The response in idling periods are more affected by the foundation stiffness and damping than the response during production, which is primarily influenced by aerodynamic damping and stiffness. Therefore, the focus in this study is on idling periods in between periods of production. Some of these idling periods lasted only a few minutes, while others lasted for several days. For data used in this study, a requirement was set for a minimum idling period of 24 min, with the first and last 2 min discarded to avoid influence from start up and shut down of the turbine. Table 1 shows the analysed time periods together with information about maximum and minimum wind and wave speed.

Fig. 2 shows the distribution of the analysed time periods over wind speeds, wave heights, and wind and wave directions, described as averages in 20-min periods. The conventions for wind and wave direction are that wind is coming from an angle, and waves are moving towards an angle, see Fig. 3. The length of the red bins in the Rose diagrams corresponds to the number of 20-min periods with this observation, e.g. about fifty 20-min periods with wind direction between 27° and 36°. There is no clear dominating load direction if all measurement periods are considered. However, if only data related to time periods with statistical wave height over 1.75 m are considered, wind and wave loads in the North-South, y-direction are dominating, which results in acceleration in the y-direction and bending moment around x-axis.

3.1. Transformation to fore-aft and side-side local coordinate system

The response of an OWT is directional dependent due to the thrust on the rotor [3], i.e. there may be a small difference in the natural frequencies in the yaw direction (fore-aft) and perpendicular to yaw direction (side-side). The two directions can be analysed separately by transforming the measured accelerations and bending moments to a local coordinate system determined by the nacelle direction. Measured acceleration and strain in the global x-y coordinate system are transferred to the local coordinate system using the following equation.

$$\begin{bmatrix} side-side \\ fore-aft \end{bmatrix} = \begin{bmatrix} \cos\theta & -\sin\theta \\ \sin\theta & \cos\theta \end{bmatrix} \begin{bmatrix} X \\ Y \end{bmatrix}$$

where θ is the nacelle direction from North-y, see Fig. 3.

3.2. Estimation of load from measured strain

The average dynamic bending moment is calculated from measured strain by fitting a continuous stress plan (Eq (1)), which minimizes the square error, S(t), between measured and calculated strain (Eq (2)). The statical parts are subtracted from measured strain before the stress plane is fitted.

Table 1
Time periods used in the analyses.

Date	Total time idling	Conditions during idling	
		Significant wave height, Hs (m)	Wind speed, WS (m/s)
6–20 Oct 2013	20 h	0.1–2.3	0.8–4.2
20 Mar - 7 Apr 2013	12.7 h	0.7–1.4	0.8–2.5
8–11 Dec 2012	95.8 h	0.9–2.9	2.1–17.7
4–8 Dec 2013	8.2 h	0.8–2.8	0.8–26.3
30–31 Mar 2015	0.33 h	1.7–2.4	22.0–22.4

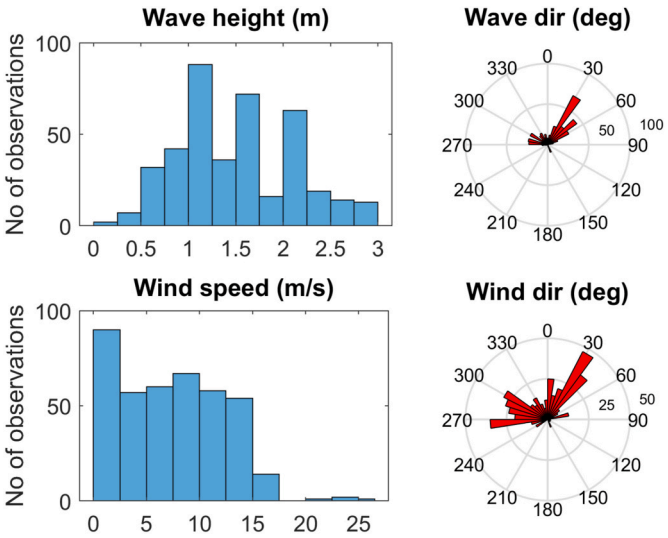

Fig. 2. Distribution of average (in 20-min periods) wind speed, wave height and wind and wave direction for the analysed time periods in Table 1.

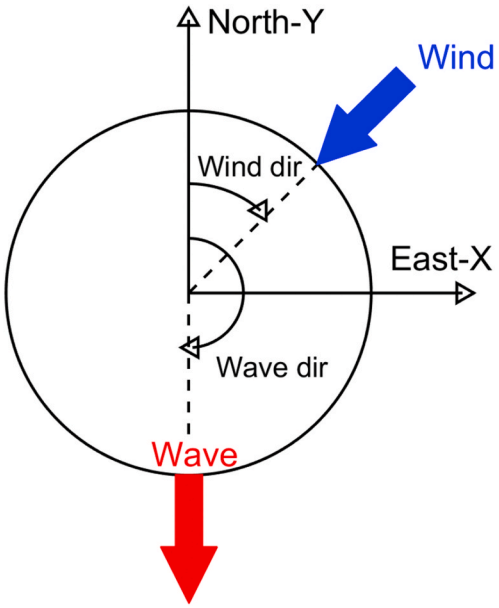

Fig. 3. Wind and wave directions, and measurement directions.

$$\varepsilon(x,y,t) = a(t)\cdot x + b(t)\cdot y \tag{1}$$

$$S(t) = \sum_{1}^{n} \left(a(t)\cdot x_i + b(t)\cdot y_i - \varepsilon_i(t)\right)^2 \tag{2}$$

Where

ε is estimated strain value, *x* and *y* are the coordinates for the strain sensors, either in a global East-West (x) North-South (y) or a local coordinate system, e.g. determined by the load direction.
a and b are constants

The dynamic bending moment is then calculated using ε(t), a(t) and b(t) that are determined as described above,

$$M(t) = \varepsilon(t) \cdot E \cdot 4 \cdot \frac{I}{D+d} \tag{3}$$

Where

E is Young's modulus = 210E6 kN/m^2 for steel, D is outer diameter of the pile (in m), d is inner diameter of the pile (in m)

4. Determination of natural frequencies

Nonparametric methods based on Fast Fourier transform (FFT) make no assumptions about the input data. Parametric and subspace methods on the other hand incorporate prior knowledge of the signal, by modelling the data as the output of a linear system driven by white noise and then attempt to estimate the parameters of that system. The advantage of these methods is that they may yield more accurate spectra with higher resolution compared to non-parametric methods. Their main disadvantage is that they require the number of components to be known in advance. In this study, Multichannel AutoRegressive Moving Average (MARMA) modelling and the MUltiple SIgnal Classification (Music) method, are used as alternative methods to FFT to determine the first natural frequencies and damping. The MARMA and Music method are described in Section 4.2. Further information about the FFT method can be found in classical textbook and references (see for example [9]).

4.1. Natural frequencies using FFT

The natural frequencies are determined using the following methodology using Fast Fourier transform (FFT):

- All idling periods with a length exceeding the 24-min criteria are divided into 20-min segments after the first and last 2 min of the idling are removed. FFT is performed on each 20-min segment using a 10-min analysis period and 50% overlap, resulting in three frequency spectra per 20-min segment, with a frequency resolution of 0.0017 Hz. Power spectral densities (PSD) are determined from the frequency spectra by averaging the three squared spectral magnitudes (variance spectra).
- To determine the overall natural frequencies, the average PSD is calculated from the PSDs of the individual time periods. Thereafter, the natural frequencies below 2 Hz are identified from the peaks in the average PSD.
- To study a possible effect of the load on the natural frequencies, the first natural frequency is determined from the PSDs from the individual 20-min segments, and plotted against average wind speed, wave height and calculated average dynamic bending moment in respective 20-min period. For this purpose, only PSDs with first natural frequency between 0.32 Hz and 0.40 Hz are used. First natural frequencies outside this range are considered to be clear outliers and not valid data.

Fig. 4 shows the overall PSD (average of PSDs from all 20-min periods) with the identified natural frequencies below 2 Hz. The first bending modes can be seen at 0.33 Hz and the second bending mode at 1.59 Hz. The peaks in between the first and second bending mode are believed to correspond to blade bending modes. The measured frequencies for the first and second bending mode in the Fore-aft direction are compared to calculated values using an aero-servo-hydro-elastic code [10] in Fig. 4. The agreement is good between the measured and calculated frequencies for the first and second natural bending mode.

Fig. 5 shows the first natural frequencies in the fore-aft and side-side directions determined from the individual 20-min segments

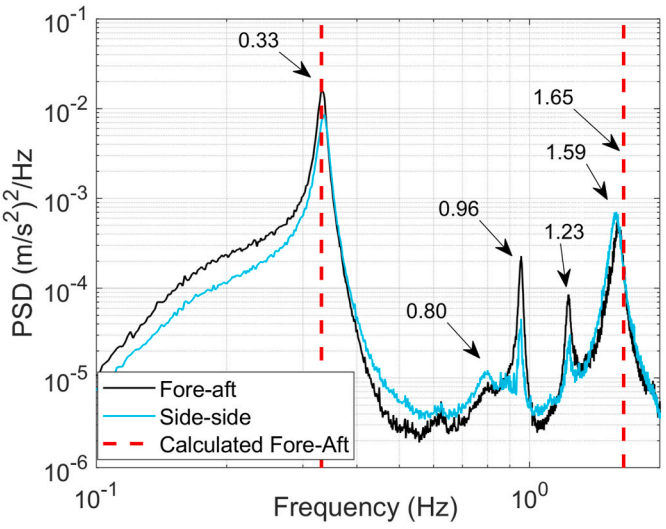

Fig. 4. Overall PSD of acceleration (average of all 20-min periods) with identified natural frequencies below 2 Hz. Calculated frequency of the first and second bending mode in the Fore-aft direction are shown for comparison.

plotted versus load parameters, namely wind speed, wave height and total dynamic bending moment. Linear fits to data are also shown. Note that the dynamic part of the bending moment is considerably lower than the total bending moment. In this study the dynamic part has been used since it shows a clearer correlation to the first natural frequency than the total bending moment.

The results indicate that the first natural frequency decreases with increased load. This is most evident for first natural frequency plotted versus the bending moment, which directly represents the load acting on the monopile. However, the spread in data is rather large and at the same time the variation in the natural frequencies with load is very small. It is therefore cruical to have a best possible frequency resolution. The frequency resolution may be improved by increasing the length of the time series used in FFT. However, since wind and wave load are changing with time the variation in load and the spread in data for each observation will at the same time increase if the length of the time series are increased. Averaging by use of overlaps, which is used to reduce the influence of noise, has the disadvantage of reducing the frequency resolution. However, various analyses have shown that neither an increase in the length of the time segments nor averaging by use of overlaps noticeably improved the results. Therefore, determination of the first natural frequency in this part of the study is based on results from FFT analysis of 20-min segments without averaging.

4.2. Alternative methods to determine first natural frequency

Two alternative methods, MUSIC in the frequency domain and MARMA in the time domain, are applied on the same time series to investigate whether it is possible to achieve better frequency resolution and damping estimates. The analyses are performed on time series from the two accelerometers (horizontal X- and Y-direction).

The MUSIC method generates an estimate of the frequency content of the signal in form of the pseudospectrum, which is determined from the signals autocorrelation matrix using Schmidt's eigenspace analysis method [11]. In this study the Matlab function *pmusic* [12] is used and the first natural frequency of the signal is determined from the peak in the obtained pseudospectrum. For the MARMA modelling a MatLab-based program is used. The program computes the covariance functions between the channels and build the corresponding block Hankel matrix. Thereafter, singular value decomposition (SVD) is used to find the singular values and corresponding vectors of the Hankel matrix. Finally, the program computes estimate of resonance periods, damping ratios and mode shapes for the expected number of modes by use of a total least square approach as described in Ref. [13]. The theory behind the program, which has been validated in several offshore concrete gravity platform design projects e.g. Ref. [14], is described in Ref. [15].

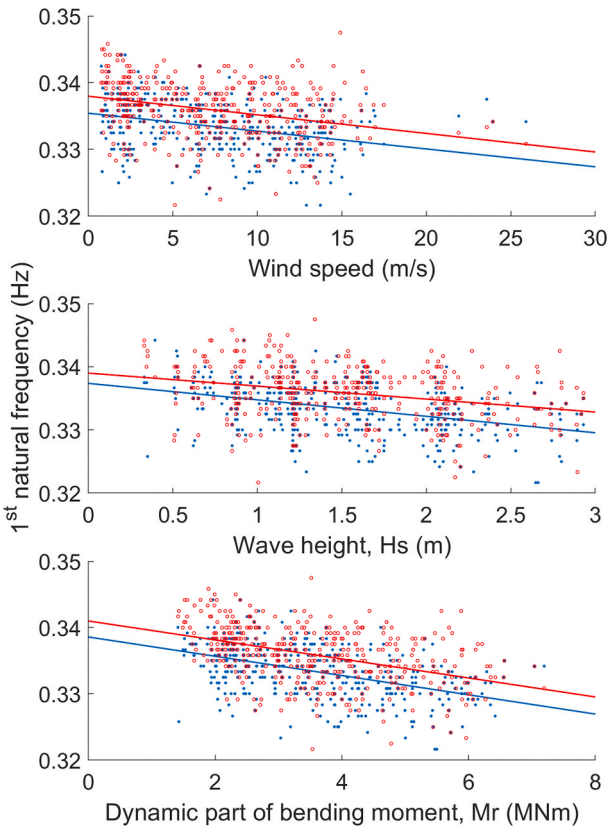

Fig. 5. First natural frequency in fore-aft (blue) and side-side (red) direction, Determined from PSD plotted against wind speed, wave height and total dynamic bending moment. (For interpretation of the references to colour in this figure legend, the reader is referred to the Web version of this article.)

In contrast to the FFT method, both MUSIC and MARMA require an initial assumption about the number of modes present in the frequency range of interest. For OWT of soft-stiff design, the number of expected modes is two in the frequency range between about 0.1 Hz and 0.5 Hz, corresponding to the closely spaced first modes in fore-aft and side-side directions. However, an initial test using different frequency resolutions showed that the Music algorithm was unable to resolve these two closely spaced modes, but when asked to find two modes, it tends to attribute the lowest mode to the peak in spectra around 0.1–0.2 Hz, which corresponds to the low frequency environmental load. Therefore, it is assumed only one mode in the Music analyses and the analyses are performed on measurement data transformed to the fore-aft, side-side coordinate system, as described in section 3.1, to supress influence from the orthogonal mode as much as possible. The MARMA method on the other hand takes advantage of cross information between channels, which makes the method much better at identifying closely spaced natural frequencies compared to spectral methods [16]. It has turned out in this study that the time series can be used without prior transformation to the fore-aft, side-side coordinate system. For the MARMA method, it is therefore assumed two modes corresponding to the first modes in the fore-aft and side-side directions.

To reduce the influence of low frequency load, e.g. wave load, and response of higher natural frequencies, a second order bandpass Butterworth filter is applied before the MARMA and Music analysis, see Fig. 6. The lower and upper cutoff frequencies of the bandpass filter are 0.1 Hz and 0.5 Hz resepectively.

Table 2 lists the overall average values of the first natural frequency in fore-aft and side-side method determined by the different methods. All three methods give relatively similar results in terms of the overall average values.

Fig. 7 shows the first natural frequencies in fore-aft and side-side directions plotted versus total dynamic bending moment and the distribution of first natural frequency, determined by the FFT, Music and MARMA method. The Music and MARMA methods clearly result in less scattered data than the FFT method. For the FFT method, the fore-aft and side-side direction seem to be mixed together, resulting in some observations of first natural frequencies being attributed to the side-side direction that probably belongs to the fore-aft direction and vice versa. The Music method on the other hand, results in less scattered data compared to the results from both the MARMA method and the FFT-method. However, like the FFT method, the Music method has problem with resolving the two modes, while the MARMA method clearly resolves the two modes.

Table 3 and Fig. 8 compare the three methods in terms of correlation between the determined fist natural frequency and the wind speed, wave height and computed dynamic bending moment. Degree of correlation are expressed by the Pearson's linear correlation coefficient. The correlation coefficient can have a value between $+1$ and -1, where $+1$ indicates total positive linear correlation, zero means no linear correlation, and -1 indicates total negative linear correlation. All three methods show a clear negative linear correlation between the first natural frequency in both directions and the wave height, wind speed and bending moment. This means that the first natural frequency decrease with increasing load, which indicates effects of soil nonlinearities because the structure is linear in the load range analysed here. The Music method gives the highest correlation in most cases.

4.3. *Changes in first natural frequency during storm events*

Another and possibly more controlled way to study the effect of load level on the overall OWT response is to study the variation of the first natural frequency with time during a storm event, from the build-up phase to the end of the declining phase. The observed first natural frequency is plotted as a function of time, together with the variations of the wave height and wind speed over the same time period and trend lines are fitted to the observations before and after the peak storm.

Fig. 9 illustrates the variation with time of the first natural frequency, determined by use of the Music method, together with wave heigh and wind speed for a storm event. The storm event include the build up phase, the peak storm period and the declining phase. The duration of the storm event is four days. The time when wind speed and wave height reach their respective maximum is about 17 h apart. Fig. 9 shows clearly that the first natural frequency decreases with increased load until the peak of the storm, and increases again

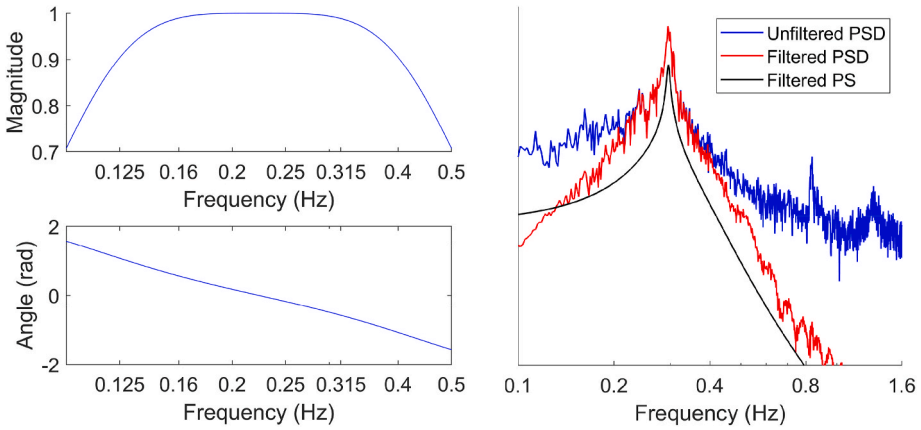

Fig. 6. Left: second order bandpass Butterworth filter with lower and higher cut-off frequencies of 0.1 Hz and 0.5 Hz right: PSD for moment around x-axis before and after bandpass filtering and pseudospectrum (PS) determined by the Music method after bandpass filtering.

Table 2
Average values for first natural frequencies (Hz) determined from all time-series calculated by the different method.

Direction	FFT	Music	MARMA
Fore-aft	0.333	0.333	0.333
Side-side	0.336	0.335	0.337

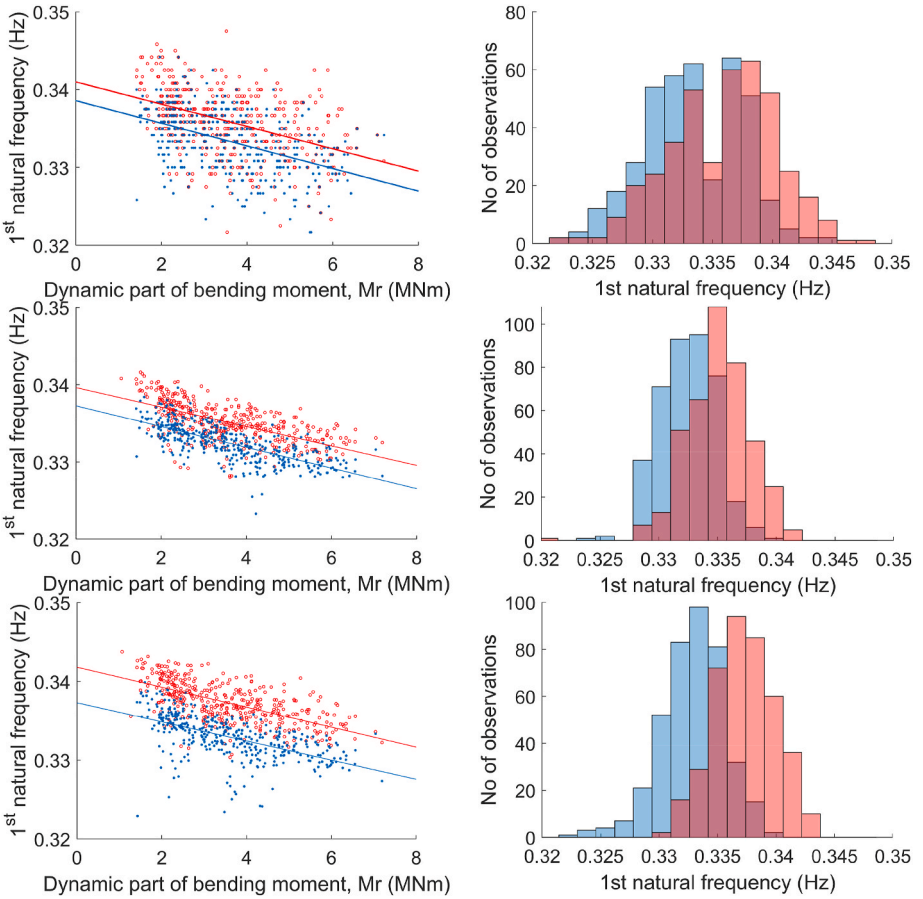

Fig. 7. First natural frequency in side-side direction (red) and fore-aft direction (blue). Left: plotted against total dynamic bending moment determined, right: distribution, top: FFT, middle: Music, bottom: MARMA. (For interpretation of the references to colour in this figure legend, the reader is referred to the Web version of this article.)

Table 3
Correlation between first natural frequency and wind speed, wave height and total dynamic bending moment.

	FFT method		Music		MARMA	
	FA	SS	FA	SS	FA	SS
Wind speed	−0.32	−0.31	−0.46	−0.43	−0.33	−0.46
Wave height	−0.39	−0.29	−0.60	−0.44	−0.43	−0.47
Bending moment	−0.47	−0.43	−0.72	−0.63	−0.57	−0.64

when waves and wind decrease. The lowest values for the first natural frequency are measured when the wave height is highest. Further, the first natural frequency increases apparently immediately when the wave height decreases, but it seems rather unaffected by the decrease in wind speed. This indicates that aerodynamic effects influence the first natural frequency to a lesser extent than possible hydrodynamic effects and soil nonlinearity.

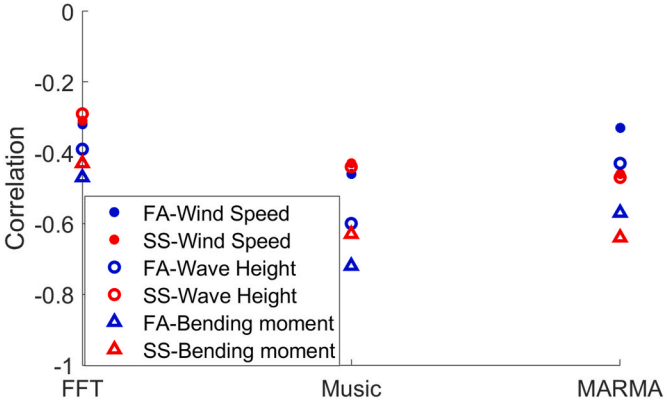

Fig. 8. Correlation between first natural frequency and wind speed, wave height and total dynamic bending moment.

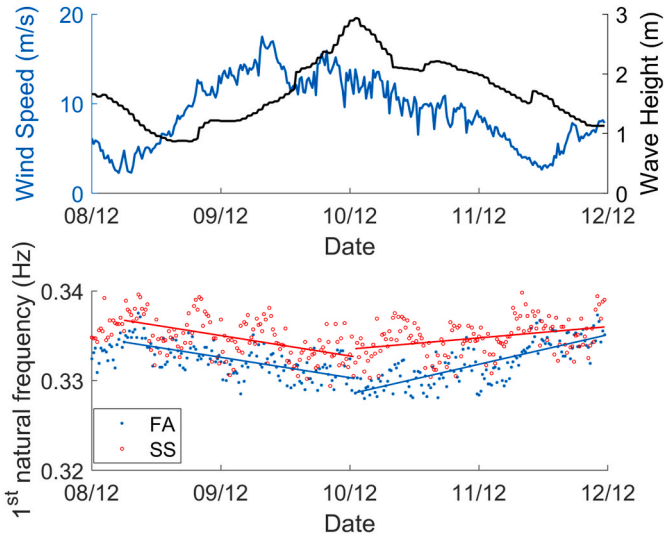

Fig. 9. First natural frequency determined by Music method versus time during storm events. Wind speed and wave height are shown for comparison.

5. Assessment of damping

Damping can be assessed from the measured data by using different methods both in the frequency domain and in the time domain. All these methods estimate the overall damping of the system, which consists of a combination of aerodynamic, structural, hydrodynamic and soil damping, together with apparent damping due to vibration-reducing devices, such as a tuned mass damper [8]. When the turbine is parked or idling the aeroelastic damping is low, and as shown in the study of the storm event, the wind speed does not seem to affect the first natural frequency.

In the frequency domain, the half-power bandwidth method can be used to estimate the damping ratio. By assuming that the damping ratio ζ is small (less than about 10%), the damping ratio can be estimated using the following equation:

$$\zeta \approx \frac{f_2 - f_1}{2f_n}$$

where f_2 and f_1 are the upper and lower half-power frequencies, and f_n is the natural frequency.

For structures with closely spaced modes possible mode coupling may lead to errors in the damping estimate [17]. For OWT structures on monopiles the first modes in the fore-aft and side-side direction are very closely spaced and a mode coupling is therefore possible. If mode coupling occurs, vibrational energy will be transferred from the highest to the lowest damped mode [2]. Damping determined with the half power bandwidth method should therefore only be considered as approximates of the real damping. Further, to obtain reasonably good estimate of the damping, it is important that the frequency resolution is fine enough for the shapes of the peaks to be correctly represented in the PSD, since a too coarse resolution will make the peaks wider and lower leading to

over-estimation of the damping. On the other hand, averaging is necessary to obtain peaks smooth enough such that the half power bandwidth method can be applied. In this study the half power bandwidth method was applied to the overall PSD calculated from all the time series as shown in Fig. 4. However, also with the obtained overall frequency resolution of 0.0017 Hz, the peaks corresponding to the first natural frequencies are not described perfectly as shown in Fig. 10. To mitigate this, a cubic spline function was fitted around the peak before determining the half-power bandwidth. As an alternative approach a single degree of freedom (SDOF) system was fitted to the measured PSD by use of least squares estimation in the frequency range from f_1 to f_2. The damping was thereafter determined from the parameters of the SDOF system. Fig. 10 shows the measured PSD, with fitted splines and SDOF-systems in the fore-aft direction together with damping ratio estimated from the half-power bandwidth method.

In the time domain, the MARMA method delivers estimated damping for each mode as a direct output. Compared to the half-power bandwidth method, the MARMA method also has the advantage that it can be applied to shorter time series, since the method only needs good covariance estimates for a small number of time-lags. However, using 20-min time segments to determine damping by the MARMA method turned out to result in a large spread in the obtained damping ratios. Therefore, 1-h long time segments are used for determination of damping with MARMA. Table 4 shows overall damping calculated as an average of all results from the half-power bandwidth method and MARMA modelling.

Compared to half-power bandwidth method, the MARMA methods results in lower difference in damping between the two directions. The estimated damping ratios in Table 4 are somewhat lower than those reported from rotor stop test in other studies. In Ref. [4] it was concluded that for the first natural frequency, a 3% damping ratio was a reasonable estimate. In Ref. [2] the authors found that the first modal damping in terms of the logarithmic decrement (δ) was in the range of 0.15–0.16, which is equivalent to 2.4–2.6% damping ratio ($\delta \approx 2\pi\zeta$). However, in Ref. [18] a damping ratio as low as 1.05% was reported for the first natural frequency from an overspeed test. For the same structure, the damping from an ambient excitation test at low wind speeds was determined to be around 0.9–1.0%. During both of these tests a tuned mass damper in top of the tower was turned off. According to Ref. [2] the damping from the tuned mass damper together with the soil damping was believed to be the biggest contributors to the total damping for offshore wind turbines on monopile foundations when aero-dynamic damping is not present. The OWT in the present study is not equipped with a tuned mass damper.

5.1. *Effect of load intensity on damping*

With the MARMA method damping can also be calculated for shorter time periods without averaging, which is not the case for the half-power bandwidth method. This allows study of the effect of load on damping. Fig. 11 shows damping at the first natural frequency determined by the MARMA method for 1-h time periods plotted against wind speed, wave height and total dynamic bending moment. The figures clearly illustrate an increase in overall damping with the excitation and a clear correlation with increased response of the system.

Table 5 shows the correlation between the determined damping at the first natural frequency by MARMA method and the wind speed, wave height and computed dynamic bending moment. Statistical significance can be proved by the p-value, which is the probability that the current result would have been found if the correlation coefficient were zero (the null hypothesis). If the p-value is lower than a certain number, the correlation coefficient is considered statistically significant. Only correlation coefficients with a corresponding p-value lower than 5% are reported in Table 5. The results indicate a small positive correlation between damping and load intensity in the side-side direction, i.e. the damping increases with increased load. The results are consistent with the negative correlation between the first natural frequency and load intensity.

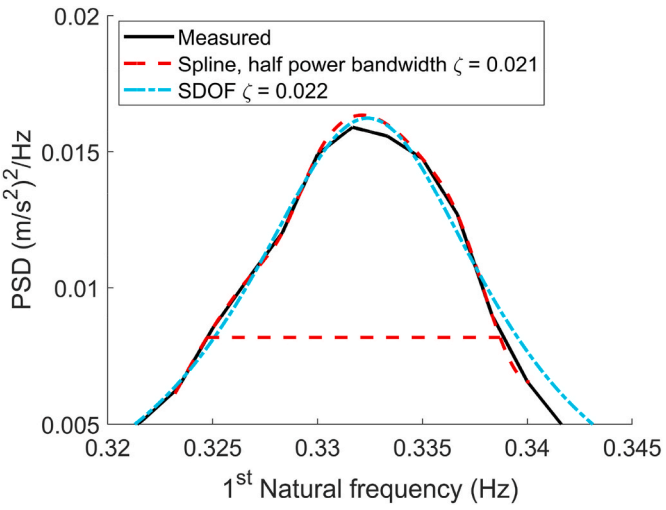

Fig. 10. Overall PSD of acceleration (average of all 20-min periods) in fore-aft direction around the first natural frequency together with fitted spline functions and SDOF system and determined damping.

Table 4
First natural frequencies (f_n) and damping ratio (ζ) determined by the half-power bandwidth method and MARMA-method.

Direction	FFT		MARMA	
	f_n (Hz)	ζ	f_n (Hz)	ζ
Fore-aft	0.333	0.020	0.333	0.020
Side-side	0.336	0.025	0.337	0.021

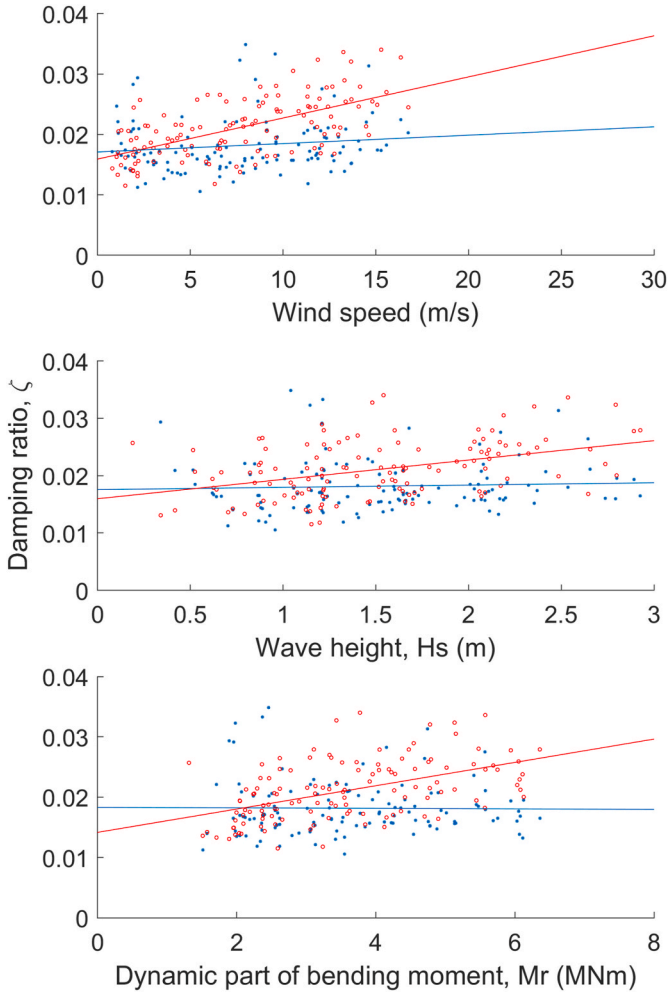

Fig. 11. Damping at first natural frequency in side-side direction (red) and fore-aft direction (blue). Determined by MARMA method and plotted against wind speed, wave height and total dynamic bending moment. (For interpretation of the references to colour in this figure legend, the reader is referred to the Web version of this article.)

Table 5
Correlation between damping at first natural frequency and wind speed, wave height and total dynamic bending moment. Only results which are statistically significant (Pval $<$ 0.05) are reported.

	FA	SS
Wind speed	–	0.62
Wave height	–	0.41
Dynamic bending moment	–	0.50

6. Dynamic parameters estimated by numerical model

Changes in the natural frequency and damping have important implications on the design and performance of OWTs. Therefore, an attempt is made here to numerically simulate the observed responses by using a dynamic soil-structure interaction (SSI) model of the measured OWT. Because, the observed changes in these two parameters are believed to be largely due the nonlinear soil response, a simple nonlinear macro-element soil spring is used as shown in Fig. 12-left following [19]. The macro-element in this case represents the nonlinear force-displacement relationships, the so-called backbone curves, of the monopile-soil system at the pile top (seabed).

Fig. 12-right display the backbone curves for the bending moment vs rotation at the pile top and horizontal force vs horizontal displacement. These curves were computed by a finite element model using an advanced nonlinear constitutive soil model [20]. The tower and transition piece are modelled by beam elements with proper masses and section properties. The nacelle and blades are modelled as one lumped mass on top of the tower, 106 m above the seabed. This means that the fore-aft and side-side direction will be identical in the model. To account for coupling between the horizontal and rotational soil springs (k_x and and k_r in Fig. 12), the model is mounted on a massless rigid link with length 4.5 m as described in Ref. [21].

Hysteretic response of the soil springs is represented by a kinematic hardening model, often referred to as Masing's rule. Fig. 13 illustrates the principles of the hysteretic response in a moment-rotation springs at different levels of moment. The area under a closed loop that reflects the lost energy in a cycle is a measure of damping. The kinematic hardening rule can readily be implemented using a series of parallel elastic-plastic springs (see for example [22] for details).

The model, as described above, is used to investigate the effect of load level on the natural frequency and overall damping and compare the results with the measured values. In order to clearly identify the role of damping from the nonlinear soil response, a Rayleigh damping ratio of 0.015 (1.5%), corresponding to the low limit of loads in Fig. 11, is assigned to the structure at frequencies equal to the first natural frequency, f_1, and at $5{\cdot}f_1$. The model is then set to a free vibration by applying a force at nacelle level and release. Fig. 14 plots the simulated time history of bending moment on top of the monopile (seabed). The peaks of this response are used to estimate the natural frequency and the logarithmic decrement is used to estimate the damping ratio, both as functions of the bending moment.

Fig. 15-left display the variations of first natural frequency with the bending moment at top of the monopile. Fig. 15-right presents the corresponding variations for the damping ratio. The first natural frequency is about 0.34 Hz at very small loads, which compares well with the measured values. At moments reaching about 10 MNm (which is the maximum value recorded during the measurements), the first natural frequency reduces to 0.339 Hz. The damping ratio starts at about 0.015 (the assigned structural damping) for small bending moments and reaches about 0.017 at 10 MNm. Although the trends are consistent with the measurements, the reduction in natural frequency and increase in damping are less than that observed in the measurements (Figs. 7 and 11 respectively), indicating contribution from other factors than soil nonlinearity, such as hydrodynamic effects. It should be noted that the uncertainties and natural variations in the measured data in the measured range do not allow an accurate assessment of the validity of the adopted numerical model. However, the general trends in the simulated data provide confidence in the model. In practice, very small damping ratios, as low as 0.5–1.0% are used in analysis and design of OWTs. The results in Fig. 15b reveal that for the case investigated in this study, the damping can increase to as high as 2% at large bending moments.

Contribution of soil damping to the overall system damping is strongly dependent on the relative stiffness of the tower and foundation. In the case studies here, the foundation is considerably stiffer than the tower structure. In more modern OWTs with smaller monopiles, the foundations are less stiff which allows them to contribute to a larger extent to the overall damping. Numerical tools such as the one presented in this study are capable of capturing the nonlinear soil response and their effect on the systems damping.

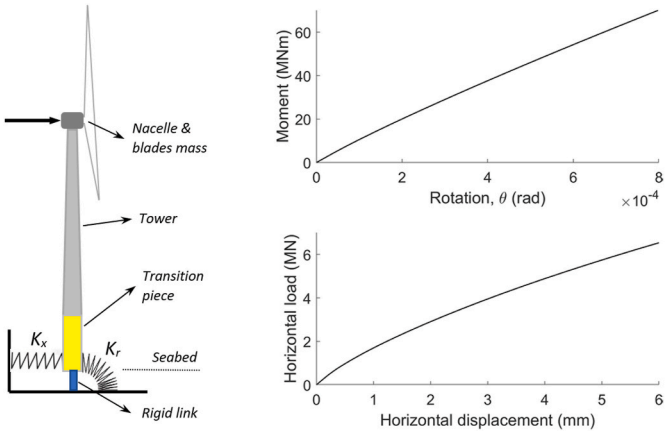

Fig. 12. Left: sketch of OWT on horizontal and rotational nonlinear spring, top right: moment-rotation relationship, bottom right: horizontal force-horizontal displacement relationship.

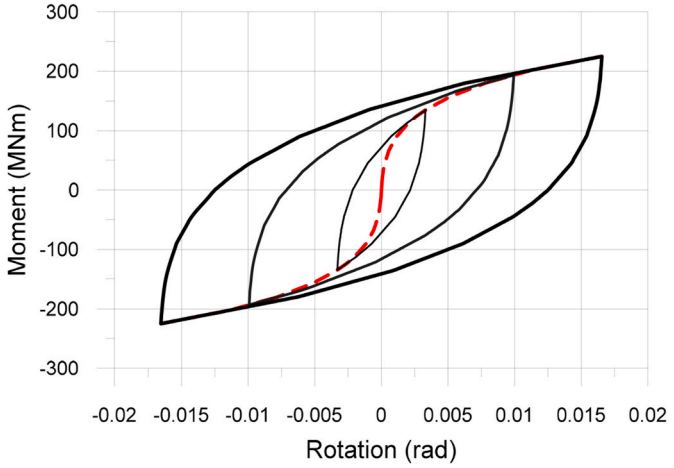

Fig. 13. Hysteretic responses at different load levels following Masing's rule.

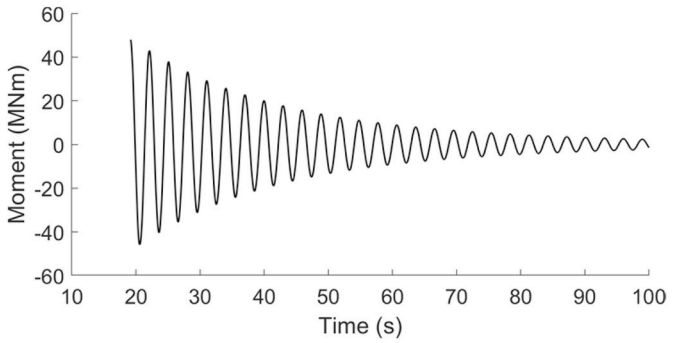

Fig. 14. Moment versus rotation at top of monopile following a free vibration numerical experiment.

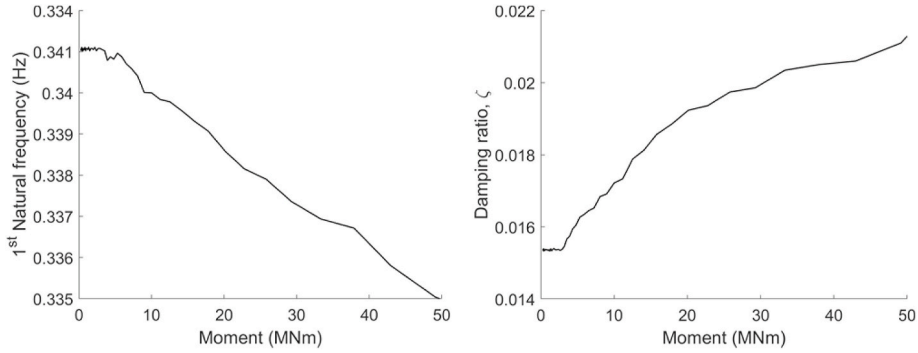

Fig. 15. Variation of natural frequency (left) and damping ratio (right) as functions of bending moment on top of pile.

7. Summary and conclusions

In this paper measured dynamic field data from a wind farm in the North Sea with monopile foundations are analysed. The ground conditions at the site are dominated by clay. Only measurement data from periods when the turbines are idling are included in the analyses. The natural frequencies and associated damping are determined using different methods in the frequency and time domain, e.g. Fast Fourier Transform (FFT), Multichannel AutoRegressive Moving Average (MARMA) modelling and MUltiple SIgnal Classification (Music).

A clear correlation is demonstrated between load level and first natural frequency for all three methods. Compared to the FFT method, the MARMA and MUSIC methods gives a better frequency resolution. The MARMA method also effectively resolves the closely

spaced modes in fore-aft and side-side direction. By using the MUSIC method to analyse measured data during a storm event, it is demonstrated that the first natural frequency decreases with increased load until the peak of the storm, and increases again apparently immediately when the waves and wind decreases.

The estimated damping ratio for time periods when the turbine is idling is about 2.0–2.5%. The estimated damping ratio is somewhat lower than reported from other field tests. The MARMA method is used to study the effect of load on damping. The results indicate a small positive correlation between damping and load, i.e. the damping increases with increased load. This is more clearly seen for the side-side mode than for the fore-aft mode.

The observed responses are simulated using a nonlinear SSI model in which the structure is represented by beam element and the monopile is represented by a nonlinear macro-element in the form of nonlinear force-displacement relationships at top of the monopile. The simulated results reproduce the general trends in the observed reduction in the first natural frequency and increased damping ratio with the load level. However, the effect of the load level is less than that observed in the measurements, indicating contribution also from other factors than soil nonlinearity.

While the uncertainties in the measured values, especially damping ratio, do not allow an accurate assessment of the simulated data, the general trends in the simulated damping values, which are solely due to the nonlinear soil springs in the adopted numerical model, indicate a satisfactory performance of the adopted soil spring model.

Declaration of competing interest

The authors declare that they have no known competing financial interests or personal relationships that could have appeared to influence the work reported in this paper.

Acknowledgements

This study was performed with support from the research project REDWIN (Reducing cost of offshore wind by integrated structural and geotechnical design), funded by the Research Council of Norway, Grant Agreement 243984. This support is highly appreciated.

References

[1] Álamo GM, Aznárez JJ, Padrón LA, Martínez-Castro AE, Gallego R, Maeso O. Dynamic soil-structure interaction in offshore wind turbines on monopiles in layered seabed based on real data. Ocean Eng 2018;156:14–24.
[2] Damgaard M, Ibsen LB, Andersen LV, Andersen JKF. Cross-wind modal properties of offshore wind turbines identified by full scale testing. J Wind Eng Ind Aerod 2013;116:94–108.
[3] Kallehave D, Thilsted CL, Troya A. Observed variations of monopile foundation stiffness. Front Offshore Geotech 2015-05-15;III:717–22.
[4] Versteijlen WG, Metrikine AV, Hoving JS, Smid E, De Vries WE. Estimation of the vibration decrement of an offshore wind turbine support structure caused by its interaction with soil. 2011. http://resolver.tudelft.nl/uuid:608f979a-d199-463e-899c-0007103cfdb0.
[5] Hald T, Mørch C, Jensen L, LeBlanc Bakmar C, Ahle K. Revisiting monopile design using p-y curves Results from full scale measurements on Horns Rev. EWEA 2009. 2009-09.
[6] Tarp-Johansen NJ, Andersen LC, Damgaard E, Mørch C, Frandsen S, Kallesøe B. Comparing sources of damping of cross-wind motion. In: European offshore wind. Conference & Exhibition The European Wind Energy Association; 2009.
[7] Shirzadeh R, Weijtjens W, Guillaume P, Devriendt C. The dynamics of an offshore wind turbine in parked conditions: a comparison between simulations and measurements. Wind Energy 2015;18:1685–702.
[8] Shirzadeh R, Devriendt C, Bidakhvidi MA, Guillaume P. Experimental and computational damping estimation of an offshore wind turbine on a monopile foundation. J Wind Eng Ind Aerod 2013;120(September):96–106.
[9] Bendat JS, Piersol AG. Random data: analysis and measurement procedures. fourth ed. John Wiley & Sons, Inc; 2010.
[10] Page AM, Næss V, De Vaal JB, Eiksund GR, Nygaard TA. Impact of foundation modelling in offshore wind turbines: comparison between simulations and field data. Mar Struct 2019;64:379–400.
[11] Marple SL. Digital spectral analysis. Englewood Cliffs, NJ: Prentice-Hall; 1987. p. 373–8.
[12] MATLAB. https://se.mathworks.com/help/signal/ug/spectral-analysis.html.
[13] Golub GH, Van Loan CF. An analysis of the total least squares problem. SIAM J Numer Anal 1980;17(6):883–93.
[14] Hoeklie M, Hansteen OE. Measured and predicted dynamic behavior of the Gullfaks A platform. In: Proceedings from 20th annual OTC Houston, May 2-5; 1988.
[15] Hansteen OE. Outline of a multichannel ARMA method to estimate resonance frequencies and associated mode spapes from recorded time histories of acceleration. NGI Rep. 51512-7 1987. NGI Rep. 51512-7.
[16] Olagnon M, Prevosto M. The variations of damping ratios with sea conditions for offshore structure under natural excitation. In: Proceedings from 16th annual OTC Houston, May 7-9; 1984.
[17] Papagiannopoulos GA, Hatzigeorgiou GD. On the use of the half-power band width method to estimate damping in building structures. Soil Dynam Earthq Eng 2011;31:1075–9.
[18] Devriendt C, El-Kafafy M, De Sitter G, Jordaens PJ, Guillaume P. Continuous dynamic monitoring of an offshore wind turbine on a monopile foundation. Proc ISMA 2012.
[19] Kaynia AM. Seismic considerations in design of offshore wind turbines. Soil Dynam Earthq Eng 2019;124:399–407. https://doi.org/10.1016/j.soildyn.2018.04.038.
[20] Page AM, Grimstad G, Eiksund GR, Jostad HP. A macro-element pile foundation model for integrated analyses of monopile-based offshore wind turbines. Ocean Eng 2018;167:23–35.
[21] Løken IB, Kaynia AM. Effect of foundation type and modelling on dynamic response and fatigue of offshore wind turbines. Wind Energy 2019;22:1667–83. https://doi.org/10.1002/we.2394.
[22] Krathe VL, Kaynia AM. Implementation of a non-linear foundation model for soil-structure interaction analysis of offshore wind turbines in FAST. Wind Energy 2017;20(4):695–712. https://doi.org/10.1002/we.2031. John Wiley & Sons, Ltd.